Numerical Calculation of Compact Torus Equilibria

D. E. Shumaker*

Lawrence Livermore National Laboratory Livermore, California 94550

A method is presented for the calculation of a MHD equilibrium for an axisymmetric compact torus. The plasma pressure is assumed to be a scalar quantity. The plasma and magnetic fields are determined by given adiabatic quantities, entropy, poloidal and toroidal magnetic flux. The equilibrium calculation proceeds by alternating between the solution of the 2-D Grad–Shafranov equation and a 1-D flux surface average of this equation. The 2-D calculation utilizes flux surface coordinates and finite elements. The poloidal flux function ψ is computed on an approximate flux surface coordinate system (χ, λ). The points describing the χ surface are moved to coincide with the surface of constant ψ. The 1-D step computes the volume enclosed by each surface. The calculation is necessary due to the equilibrium being specified by adiabatic quantities. Three examples of equilibria computed by this method are represented, two spheromaks and one field reversed configuration (FRC).

I. Introduction

A compact torus is a configuration where the plasma region extends to the axis of rotational symmetry. The magnetic field structure forms two regions divided by a separatrix, see Fig. 1. Inside the separatrix the magnetic field lines form closed nested toroidal surfaces, flux surfaces. Outside the separatrix the field lines are open. The presence of the separatrix in the region of interest is one of the features of a compact torus. A magnetic field vortex point, or o-point, is enclosed by the separatrix, see Fig. 1. The procedure given here also could be used to determine equilibrium for other axisymmetric configurations, such as, tokamaks and field reversed pinches. These equilibria calculation would be simpler since there is no separatrix in these configuration.

Numerically determined equilibria are used in conjunction with transport, compression and stability calculations. The transport calculations referred to here compute the evolution of the plasma and magnetic field by alternating between the solution of a 2-D equilibrium and a 1-D transport calculation [1]. This type of transport code is generally referred to as a $1\frac{1}{2}$D transport code [2]. Codes of this type have been used to simulate tokamak experiments [3–5].
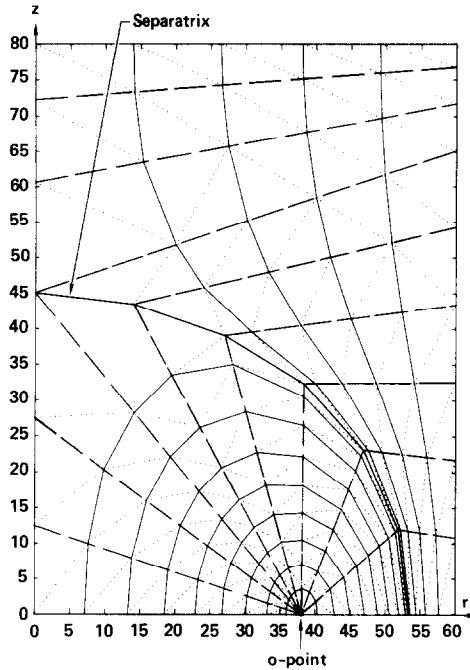
FIG. 1. χ, λ grid. Dark lines are surfaces of constant χ. Dashed lines are surfaces of constant λ. Dotted lines denote boundary of finite elements.

Other possible uses of the code described here are adiabatic compression studies and initialization of MHD stability calculations. Since adiabatic quantities are used to specify the equilibrium, compression studies can be made by computing a series of equilibria with different boundary conditions. Compression of compact toroids can be done by flux compression or wall compression [6]. Numerical equilibria are useful in MHD stability calculations as initial conditions for fast time scale evolution codes. Also, some stability critera [4] involve integrals over equilibrium flux surfaces.

The equilibrium code described in this paper was developed as a replacement for the equilibrium calculation used in the transport code described in [1]. The equilibrium calculation described there uses an r, z grid. The use of this grid makes the evaluation of flux surface integrals difficult since 2-D interpolation must be used to follow the magnetic flux surface on the r, z grid. The equilibrium calculation described in this paper uses flux surface coordinates, which makes the evaluation of surface integrals faster and more accurate. Also the use of this coordinate system does not require as many grid points in the 2-D grid, thus reducing the computational time. This is due, in part, to the ability to concentrate the points in the region where the flux surface curvature is high. Also the surface integrals which are required during the equilibrium calculation can be computed with more uniform accuracy, since there are the same number of points on each surface. Other methods which use an r, z grid have problems computing flux surface integrals near the o-point

since the flux surfaces are small and may encompass only a few grid points. Equilibria have been computed for tokamaks using flux surface coordinates [7]. Also tokamak transport codes have used flux surface coordinates in the equilibrium calculations [3].

In the calculation described in this paper the equilibrium is specified by adabatic quantities. The main reason for using this method is that they are used in the transport code described in [1]. The basic method for computing an axisymmetric equilibrium when adiabatic quantities are used has been given by Grad [2]. In an axisymmetric plasma with scalar pressure it can be shown that the plasma pressure P is a function of ψ, the poloidal magnetic flux function [8]. Also the toroidal magnetic flux function f defined by

$$f = rB_T \tag{1}$$

is a function of ψ only [8], r is the distance from the axis of rotational symmetry. The magnetic field is given by

$$\mathbf{B} = \nabla\psi \times \nabla\theta + f\nabla\theta, \tag{2}$$

where θ is the toroidal angle. The ψ function is described by the Grad–Shafranov equation,

$$\nabla \cdot \left(\frac{\nabla\psi}{r^2}\right) = -4\pi \frac{dP}{d\psi} - \frac{1}{2r^2}\frac{df^2}{d\psi}. \tag{3}$$

There are basically two methods to specify a solution to Eq. (3). One is to specify the functions on the right-hand side, that is, $P(\psi)$ and $f(\psi)$. An alternate method, which is used in the calculations presented here, is to specify some adiabatic quantities. A set of adiabatic quantities which is used in this calculation consist of specifying two adiabatic functions, Q_p and Q_f, and the range of the ψ function. The range of the ψ function is determined by giving the o-point value ψ_o and the value at the outer boundary ψ_w. The separatrix is defined as the $\psi = 0$ surface. One of the adiabatic functions which is used here is proportional to the entropy enclosed by adjacent flux surfaces.

$$Q_p = PS_1^{5/3}. \tag{4}$$

This will be called the entropy function. The function S_1 is given by

$$S_1 = \int \frac{d^2r}{|\nabla\rho|} = \frac{d}{d\rho}\int d^3r = \frac{dV}{d\rho}, \tag{5}$$

where V is the volume enclosed by a flux surface labeled by ρ. The volume integral is over the volume enclosed by the flux surface. And the surface integral is over the flux surface, where ρ is a dimensionless independent variable

$$\rho = \frac{\psi_o - \psi}{\psi_o}. \tag{6}$$

Given $Q_p(\rho)$ and $S_1(\rho)$ the pressure $P(\rho)$ can be obtained from Eq. (4). The other adiabatic function which determines the toroidal magnetic flux is given by

$$Q_f = fS_2 = -\psi_o 4\pi^2 q, \tag{7}$$

where q is the magnetic stability safety factor, and S_2 is given by

$$S_2 = \int \frac{d^2r}{|\nabla\rho|} \frac{1}{r^2} = \frac{d}{d\rho} \int \frac{d^3r}{r^2}. \tag{8}$$

This integral has a singularity at $\rho = 1$, because the separatrix goes to $r = 0$. This integral is evaluated by summing the volumes enclosed by the grid cells between two adjacent surfaces using the average of r for the cell to evaluate the $1/r^2$. This approximation to $1/r^2$ is inaccurate near $r = 0$, however, everywhere $1/r^2$ appears in this calculation it is multiplied by f which must be proportional to r^2 near $r = 0$. Thus the combination f/r^2 will not have a singularity.

To complete the specification of the equilibrium some type of boundary condition in the r, z plane must be specified. In this code this is done by assuming that the outer flux surface is fixed. Two types of boundary conditions can be used on the part of the boundary which is intersected by open field lines. The first is to assume that the ends of the flux surfaces are fixed. This is the appropriate boundary condition if the open field lines pass into a conductor. The other type of boundary condition which can be used here is to assume that the field lines become parallel to the z axis, $\partial\psi/\partial z = 0$, at this boundary.

The equilibrium calculation consists of two parts, a 2-D solution of the Grad–Shafranov equation using finite elements in the flux surface coordinate system, described in Section II. The other part of the calculation is the solution of the 1-D flux surface averaged Grad–Shafranov equation which is described in Section III. Section IV describes the coupling of the two parts of the calculation. In Section V three examples of equilibria calculated by this method are presented.

II. SOLUTION OF THE GRAD–SHAFRANOV EQUATION ON THE χ, λ GRID

This section will describe the 2-D aspects of the equilibrium calculation. The 2-D calculation alternates with the 1-D calculation which will be described in the next section. The 1-D calculation provides the information needed on the right-hand side of Eq. (3), that is, $P(\rho)$ and $f(\rho)$.

To start the calculation an initial χ, λ grid must be set up, that is, the arrays $r(\chi_j, \lambda_l)$ and $z(\chi_j, \lambda_l)$ must be initialized. This is done by guessing at the positions of the flux surface or inputting a grid from a previous calculation. The χ, λ coordinate system used here is not orthogonal. The distribution of the λ_l points on each χ_j surface is somewhat arbitrary, however a smooth distribution of points produces better results. The procedure used here starts by positioning the points on the separatrix and the outer flux surface, fixed conductor. The λ_l points on the remaining

χ_j surfaces are positioned so that the λ_l points form a straight line. An example of a grid generated in this manner is shown in Fig. 1. The χ_j need not be evenly spaced. Better results are obtained if the χ_j are adjusted so that there are more χ_j surfaces near the o-point and separatrix. In this calculation the plasma and magnetic fields are assumed to be symmetric about $z = 0$. Thus the grid is only set up in half of the r, z space.

A finite element method is used to compute ψ on the χ, λ grid. Each quadrilateral of the grid is divided into two triangles. There are two possible ways of dividing each quadrilateral into triangular finite elements. The computer code determines which opposite corners of the quadrilateral are closest and connects these corners from the two triangles. This procedure produces two triangles with the least amount of elongation. This procedure is done each time the grid points are repositioned. Thus each grid point can be connected to as many as eight neighboring points and as few as four. The ψ function in each element is described by a simple three parameter linear function of r and z.

If N_{jl} is the shape function for the χ_j, λ_l point, then the ψ function is approximated by

$$\psi = \sum_{jl} \psi_{jl} N_{jl}. \tag{9}$$

Each N_{jl} has four to eight parts which are each linear function of r and z; N_{jl} has the value 1 at (χ_j, λ_l) and zero at all other grid points.

A Galerkin [9] method is used to obtain a matrix equation for the unknown ψ_{jl}. The Grad–Shafranov equation (3) is multiplied by each of the N_{jl} and integrated over the region of nonzero N_{jl}. As usual the left-hand side of this equation is integrated by parts to remove the second derivatives and replace them with products of two first derivatives. The resulting set of equations have the following matrix form

$$\mathbf{A}\boldsymbol{\psi} = \mathbf{B}. \tag{10}$$

The vector $\boldsymbol{\psi}$ contains the unknowns ψ_{jl}. Since each surface has the same number of points and each point (j, l) is only connected to the $l - 1$, l, and $l + 1$ points on the $j - 1$, j, and $j + 1$ surface, the matrix $\mathbf{A}$ has nine bands. The grid was set up in this way to make use of fast matrix inverters which exist for a nine banded matrix. The elements of the bands are,

$$a_{1,k} = -\int \frac{d^3 r}{r^2} \nabla N_{jl} \cdot \nabla N_{j-1,l-1},$$

$$a_{2,k} = -\int \frac{d^3 r}{r^2} \nabla N_{jl} \cdot \nabla N_{j-1,l},$$

$$a_{3,k} = -\int \frac{d^3 r}{r^2} \nabla N_{jl} \cdot \nabla N_{j-1,l+1},$$

$$a_{4,k} = -\int \frac{d^3 r}{r^2} \nabla N_{jl} \cdot \nabla N_{j,l-1},$$

$$a_{5,k} = -\int \frac{d^3r}{r^2} \nabla N_{jl} \cdot \nabla N_{jl},$$

$$a_{6,k} = -\int \frac{d^3r}{r^2} \nabla N_{jl} \cdot \nabla N_{jl+1},$$

$$a_{7,k} = -\int \frac{d^3r}{r^2} \nabla N_{jl} \cdot \nabla N_{j+1,l-1},$$

$$a_{8,k} = -\int \frac{d^3r}{r^2} \nabla N_{jl} \cdot \nabla N_{j+1,l},$$

$$a_{9,k} = -\int \frac{d^3r}{r^2} \nabla N_{jl} \cdot \nabla N_{j+1,l+1}, \tag{11}$$

where $k = (j-1)L + l$, and L is the number of points on each χ surface. The elements of the B vector are,

$$b_k = -4\pi \int d^3r N_{jl} \frac{dP}{d\psi} - \frac{1}{2} \int \frac{d^3r}{r^2} N_{jl} \frac{df^2}{d\psi}. \tag{12}$$

An incomplete Cholesky conjugate gradient (ICCG) method [10] is used to solved the matrix equation (10). An iterative method is more compatible with this problem since the solution of the linear matrix equation (10) is only one step in the overall iteration (between 1-D and 2-D equation). It is time consuming and unnecessary to have a very accurate solution to Eq. (10) at every iteration. Error parameters and iteration limits which are input parameters for the ICCG subroutines are used to control the number of iterations in the solution of Eq. (10). As the overall iterations converge the number of iterations in the ICCG part will become smaller. This is due to the fact that the initial guess at ψ used by the ICCG method is closer to the answer.

In some equilibrium calculations it becomes difficult to solve Eq. (10). This is particularly true of the highly elongated FRC equilibrium. In order to accelerate the convergence of the ICCG method some damping is introduced into Eq. (10). This is done by adding an identity matrix times a small quantity to the left-hand side and an identity matrix times a small quantity and ψ_{jl}^{last} to the right-hand side, where ψ_{jl}^{last} is the ψ_{jl} obtained at the last 2-D solution. This procedure is equivalent to introducing an artificial time dependence in Eq. (10).

In order to preserve the nine banded structure of the matrix **A** at the o-point, the o-point is represented by L points as the other surfaces. Based on the observation that as one approaches the o-point the coupling of the point in the λ direction becomes large due to the close spacing, a strong artificial second derivative in the λ direction is added to the problem at the o-point only. This method can be checked by noting if the values of $\psi_{1,l}$ are approximately the same.

The region of the calculation in the χ, λ space is shown in Fig. 2. χ ranges from χ_o, the o-point, to χ_w, the outer flux surface. The separatrix is χ equal to zero. The λ
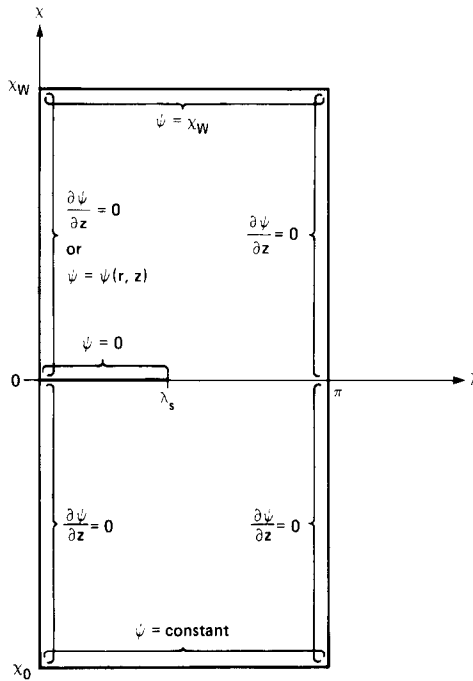
FIG. 2.   Boundary condition used on χ, λ grid for $2 - D$ calculation.

variable ranges from zero to π. The o-point corresponds to the lower boundary in this figure which is at χ_o. The ψ function will be approximately a constant along this boundary as described earlier. The left-hand boundary of Fig. 2 below $\chi = 0$ corresponds to the line from the o-point inward to $r = 0$ at $z = 0$. The boundary condition which is applied here is that $d\psi/dz = 0$. The left-hand boundary of Fig. 2 above $\chi = 0$ corresponds to the top boundary of the r, z grid, Fig. 1. There are two types of boundary conditions which can be applied here. One is $\partial\psi/\partial z = 0$. The other type is to fix ψ along this boundary. This corresponds to the problem where the magnetic field lines pass into a rigid conductor. The top boundary of Fig. 2 corresponds to the outer flux surface in the problem, it is assumed to be fixed and have a constant value of ψ_w. The right-hand side of Fig. 2 corresponds to the line form the o-point to the outer flux surface along $z = 0$. The boundary condition which is applied here is the symmetry condition $\partial\psi/\partial z = 0$.

The separatrix, $\chi = 0$ can be divided into two lines in the r, z space, the outer curved line which end at $r = 0$, and the line $r = 0$. The boundary condition $\psi = 0$ is applied on the $r = 0$ line. In the χ, λ space this boundary condition is applied by setting $\psi = 0$ on the line from 0 to λ_s at $\chi = 0$. There are no boundary conditions applied to the curved part of the separatrix. Its ψ value will become zero as the computation converges.

The next step after the ψ's have been computed on the χ, λ grid is the repositioning

of the grid points in r, z. The new minimum value of ψ, o-point, is now determined. This minimum will be at $z = 0$. The minimum ψ and its r position are determined by quadratic interpolation. The new ψ_o will not be exactly the specified value χ_o. The difference between these two quantities can be used as a measure of convergence or a check of the accuracy of the equilibrium. The ψ values inside the separatrix are scaled so that the new ψ at the o-point has the desired value.

Two different procedures are used to reposition the grid points. If the new o-point is too far from its previous position, an attempt to move the points along the λ lines will scramble the points near the o-point. The procedure which is used in this case is to move all the points in the r direction in order to place the o-point at the interpolated ψ minimum. If the o-point position is near the old position then the following procedure is used to reposition the points. The points are moved along a line of constant λ to form a more accurate ψ surface. From a line of given λ_l the r positions form a function $r(\psi_{jl})$, and the z positions form $z(\psi_{jl})$. The new values of r and z of a grid point are found by linear interpolation. This is done on each λ_l line and for each point, also the new o-point position is placed at the interpolated ψ minimum.

In order to damp oscillations which occur in some calculations during the 1-D 2-D iterations and ensure convergence, it was found that the ψ value used to determine the new position of a grid point ψ_{jl}^* should be obtained by mixing ψ_{jl} and χ_j,

$$\psi_{jl}^* = \alpha\psi_{jl} + (\alpha - 1)\chi_j. \tag{13}$$

For the FRC equilibria α must be about 0.3.

Once the points have been repositioned along the λ lines to form new flux surfaces some steps must be taken to ensure a smooth distribution of points on each χ surface. This procedure consists of moving the points along the separatrix so that the points have a smooth distribution. Then the points on the other surfaces are moved parallel on the flux surface so that the lines of constant λ are straight. Thus the lines of constant λ inside the separatrix will form straight lines from the separatrix to the o-point, and outside the separatrix from the separatrix to the outer surface. Thus a new 2-D χ, λ grid has been produced in which the χ surfaces are closer to being surfaces of constant ψ.

III. Solution of the Surface Averaged Grad–Shafranov Equation

The 1-D flux surface-averaged Grad–Shafranov equation is need to compute S_1 which is needed to compute the new values of P from Q_p and f from Q_f. The 1-D equation is a second order ODE for V the volume as a function of ρ. Its derivation and solution will be described in this section.

To perform the surface averaging of the Grad–Shafranov equation the same shape functions are used as was used in the 2-D problem. The Grad–Shafranov equation is multiplied by the sum of all the shape functions N_{jl} with the same j, and integrated

over the volume. This procedure of deriving the 1-D equation ensures consistency between the 1-D and 2-D equations. The resulting equation is,

$$\int d^3 r \nabla \left(\sum_l N_{jl} \right) \cdot \frac{\nabla \psi}{r^2} = 4\pi \int d^3 r \sum_l N_{jl} \frac{dP}{d\psi} + \frac{1}{2} \int \frac{d^3 r}{r^2} \sum_l N_{jl} \frac{df^2}{d\psi}. \qquad (14)$$

Putting in P and f in terms of Q_p and Q_f yields the tridiagonal equation for V_j,

$$a_j V_{j-1} + b_j V_j + c_j V_{j+1} = 0, \qquad (15)$$

where

$$a_j = \frac{\psi_o^2}{\Delta \rho_{j-1/2} S_{1,j-1/2}^2} K_{j-1/2} + \frac{S_{6,j} Q_{P,j-1/2}}{\Delta \rho_{j-1/2} S_{1,j-1/2}^{8/3}} + \frac{S_{7,j} Q_{f,j-1/2}^2 \bar{R}_{j-1/2}^4}{\Delta \rho_{j-1/2} S_{1,j-1/2}^3}, \qquad (16a)$$

$$c_j = \frac{\psi_o^2}{\Delta \rho_{j+1/2} S_{1,j+1/2}^2} K_{j+1/2} + \frac{S_{6,j} Q_{P,j+1/2}}{\Delta \rho_{j+1/2} S_{1,j+1/2}^{8/3}} + \frac{S_{7,j} Q_{f,j+1/2}^2 \bar{R}_{j+1/2}^4}{\Delta \rho_{j+1/2} S_{1,j+1/2}^3}, \qquad (16b)$$

$$b_j = -a_j - c_j, \qquad (16c)$$

where

$$\bar{R}_{j+1/2}^2 = \frac{S_{1,j+1/2}}{S_{2,j+1/2}}, \qquad (17)$$

$$S_{6,j} = \frac{4\pi}{\Delta \rho_j} \int d^3 r \sum_l N_{jl}, \qquad (18)$$

$$S_{7,j} = \frac{1}{2\Delta \rho_j} \int \frac{d^3 r}{r^2} \sum_l N_{jl}, \qquad (19)$$

where

$$\Delta \rho_j = \rho_{j+1/2} - \rho_{j-1/2}. \qquad (20)$$

The above integrals are over the region of nonzero N_{jl}. The four quantities, $K_{j+1/2}$, $\bar{R}_{j+1/2}^2$, $S_{6,j}$, and $S_{7,j}$ are assumed to be a constant during the calculation of V, they are obtained from the 2-D grid. The other function in Eq. (16) is

$$K_{j+1/2} = \frac{S_{1,j+1/2}}{\Delta \rho_{j+1/2}} \int d^3 r \frac{|\nabla \rho|^2}{r^2}. \qquad (21)$$

The integral in (21) is Grad's inductance, it is over the volume between surfaces ρ_{j+1} and ρ_j. $S_{1,j+1/2}$ is given by

$$S_{1,j+1/2} = \frac{V_{j+1} - V_j}{\Delta \rho_{j+1/2}}, \qquad (22)$$

where

$$\Delta\rho_{j+1/2} = \rho_{j+1} - \rho_j \tag{23}$$

and V_j is the volume enclosed by the ρ_j surface. Equation (15) is the form used in the case when the $\partial\psi/\partial z = 0$ boundary condition is used on the top boundary in the r, z space. If the rigid conductor boundary condition is used, then there will be an additional term in Eq. (15) due to a surface integral over the top boundary.

Equation (15) is soved in two separate regions. In this calculation there can be plasma in both regions, inside the separatrix and between the separatrix and outer wall. The first region is for $0 < \rho < 1$ (region enclosed by separatrix). The boundary conditions for this region is that $V(0) = 0$ and $V(1) = V_S$, where V_S is the volume enclosed by the separatrix; V_S is obtained form the 2-D solution. The second region is $1 < \rho < \rho_w$ (region between separatrix and outer flux surface). The boundary conditions for this region are $V(1) = V_S$ and $V(\rho_w) = V_w$, where V_w is the volume enclosed by the outer flux surface, which is a constant.

Since the coefficients a_j, b_j, and c_j is Eq. (15) depend on V_j through $S_{1,j+1/2}$, an iteration method must be used to solve this equation. The coefficients a_j, b_j, and c_j are determined using the last values of $S_{1,j+1/2}$. The equation is then solved for V_j which from Eq. (22) gives new values of $S_{1,j+1/2}$. Now new a_j, b_j, and c_j can be computed, and Eq. (15) can be solved again. During this iteration the quantities $K_{j+1/2}$, $\bar{R}^2_{j+1/2}$, $S_{6,j}$, and $S_{7,j}$ are held fixed. These quantities come from the 2-D solution.

With V_j determined by solving Eq. (15), the $S_{1,j+1/2}$ can be computed from Eq. (22); $S_{2,j+1/2}$ is obtained from Eq. (17) by assuming $\bar{R}^2_{j+1/2}$ does not change during the 1-D calculation. Thus P and f can be obtained from Eqs. (4) and (7). The terms on the right-hand side of the 2-D equation (3) can now be determined.

IV. SUMMARY OF 1-D 2-D ITERATION PROCEDURE

The calculation starts with the specification of the Q_p and Q_f functions and the values of ψ at the o-point and the outer wall. An initial grid is generated or read in from a previous calculation. Next the flux surface average quantities which are need for the 1-D calculation are computed. These are $K_{j+1/2}, S_{6,j}, S_{7,j}$, and $\bar{R}^2_{j+1/2}$ which are determined from the 2-D grid. Then Eq. (15) is solved for V_j. This calculation gives a better value of $S_{1,j}$ and $S_{2,j}$ which are used to compute P_j and f_j for the right-hand side of the 2-D Grad–Shafranov equation.

The 2-D equation (10) is now solved for ψ_{jl} on the χ, λ grid. The points are then moved to a new approximate ψ flux surface. Then the grid points are moved parallel to the flux surfaces to maintain a smooth distribution of points on each flux surface.

With a new grid set up the first iteration is completed and the surface integrals, $K_{j+1/2}, S_{6,j}, S_{7,j}$, and $\bar{R}^2_{j+1/2}$, can be computed. The 1-D 2-D iteration continues until a convergence criterion is satisfied. When the average value of the grid point

displacement is less than some small quantity the equilibrium is assumed to be con-
verged.

The repositioning of the x-point, where the separatrix goes to $r = 0$, can lead to
slow convergence in some cases, in particular, the elongated FRC. For these cases it
was found that adding another step in this calculation can produce better
convergence. This step consists of minimizing the total energy of the system with
respect to a displacement in the z direction of the x-point. The displacement which
was chosen has the form

$$
\delta(r, z) = \begin{cases} \delta_s[1 - (r/r_w)^2]\, z/z_s & \text{for} \quad z < z_s \\[2mm] \delta_s[1 - (r/r_w)^2]\, \dfrac{(z_t - z)}{(z_t - z_s)} & \text{for} \quad z > z_s \end{cases}. \tag{24}
$$

This displacement is δ_s for the x-point and reduces lineary to zero at $z = 0$ and at the
top, $z = z_t$. It also reduces quadratically to zero at the wall radius r_w.

The energy integral which is minimized is

$$
W = \int d^3 r \left(\frac{B^2}{8\pi} + \frac{3}{2} P \right), \tag{25}
$$

where the integral is over the entire region of the calculation. W can be assumed to be
of the form

$$
W = W_0 + \delta_s \left(\frac{dW}{d\delta} \right)_{\delta = 0} + \frac{1}{2} \delta_s^2 \left(\frac{d^2 W}{d\delta^2} \right)_{\delta = 0}, \tag{26}
$$

where W_0 is the energy integral before this displacement, $\delta = 0$. The first and second
derivatives are computed numerically by evaluating the integral (25) at $\delta_s = +\varepsilon, 0,$
and $-\varepsilon$, where ε is some small number and using finite differences to compute the
derivatives. Taking $d/d\delta_s$ of Eq. (26) and setting it to zero will yield the δ_s which
minimizes the energy, this is

$$
\delta_s = \frac{- \left(\dfrac{dW}{d\delta} \right)_{\delta = 0}}{\left(\dfrac{d^2 W}{d\delta^2} \right)_{\delta = 0}}. \tag{27}
$$

With δ_s now given, each point in the grid is now moved in the z direction by the
amount given by Eq. (24). This procedure is only used for the more difficult FRC
equilibrium. In these cases it is done every 1-D 2-D iteration.

V. Results

As a check of the accuracy of this procedure a Hill vortex solution was used as a
test case. This analytic equilibrium is given in [16]. In this test case the separatrix is

assumed to be fixed, and only the equilibrium inside the separatrix is computed. For this equillibrium the pressure P is a linear function of ψ and f is assumed to be zero. The input for this equilibrium calculation Q_p must be numerically computed. The volumes enclosed by the analytic ψ function are first numerically computed, using enough points to ensure that the error in the volumes are much less than the expected error in the equilibrium calculation. With the volumes computed the $S_{1,j+1/2}$ can be computed and with the given analytic P function Q_p, the input for the equilibrium calculation, can be determined.

After the code has computed an equilibrium the ψ_{jl} can be compared to the analytic ψ at each grid point. Four cases with spherical separatrix were run with different grid sizes. The four cases were $(J = 5, L = 10)$, $(J = 10, L = 20)$, $(J = 20, L = 40)$, and $(J = 40, L = 80)$, where J is the number of flux surfaces and L is the number of points on each flux surface. The average errors in ψ for these cases were 1.4%, 0.41%, 0.12%, and 0.033%, respectively. The maximum errors in ψ for these cases were 4.0%, 1.08%, 0.35%, and 0.090%, respectively. The number of 1-D 2-D iterations for these cases were 4, 4, 7, and 17, respectively. The Cray-1 computer time for these cases were 0.1, 0.3, 2.0, and 35.0 sec, respectively.

Oblate and prolate Hill vortex solutions were also tested. An oblate case with separatrix radius at $z = 0$ of 50 cm and separatrix z of 10 cm at $r = 0$ gave accuracy very similar to the spherical cases. No damping was required to obtain convergence in the spherical or oblate cases, however, a prolate cases which was tested required some damping to obtain convergence. This case had a separatrix radius at $z = 0$ of 10 cm and a separatrix z at $z = 0$ of 50 cm. The errors for the prolate cases were about twice that of the spherical cases.

Three equilibrium calculations are presented in this section. These examples are of current experimental devices. Compact toroids can be divided into two types, spheromaks and field reversed configurations (FRC). Spheromaks are characterized by containing both poloidal and toroidal magnetic fields which are of approximately the same order of magnitude. FRC's contain only poloidal fields. Two equilibrium calculation examples of spheromaks are presented and one of a FRC.

Figure 3a shows the contours of constant ψ for an equilibrium similar to the one produced in the CTX experiment [11]. In this equilibrium the separatrix is assumed to lie on the flux conserver which is made of copper. There is no external or guide magnetic field in this example. This plasma is produced by a magnetized coaxial plasma gun [12]. The plasma is injected into the flux conserver along the z axis through a hole in flux conserver (at $z = 20$ in Fig. 3a). This hole is not represented in this calculation.

Figure 3b is a plot of the plasma pressure at $z = 0$, Fig. 3c is a plot of the toroidal current at $z = 0$, Fig. 3d is a plot of the poloidal magnetic field at $z = 0$, and Fig. 3e is a plot of the toroidal magnetic field at $z = 0$. The poloidal magnetic field at $r = 0$, $z = 0$ has a value of -2.2 kG. The o-point radius is at 24.0 cm.

In this calculation there are 9 flux surfaces with 20 points on each flux surface for a total of 180 points in the 2-D grid. This calculation took 17 1-D 2-D iteration for a total of approximately 1.2 sec on the Cray-1 computer.
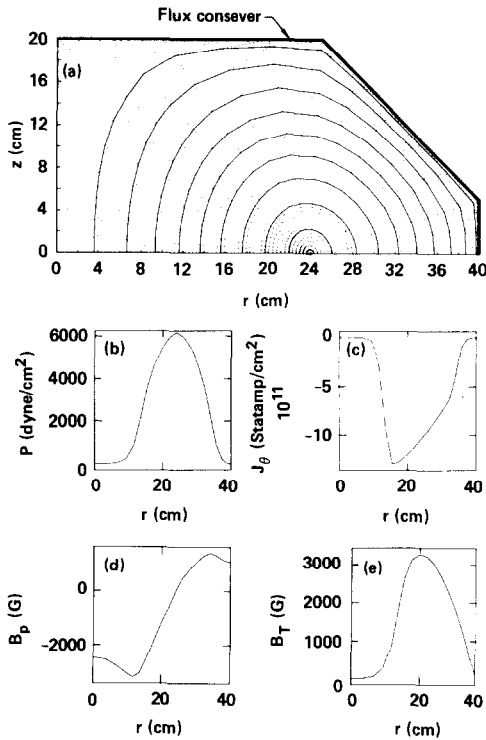
FIG. 3. CTX equilibrium, (a) χ, λ grid, (b) pressure vs. r ar $z = 0$, (c) toroidal current vs. r at $z = 0$, (d) poloidal magnetic field vs. r at $z = 0$, (e) toroidal magnetic field vs. r at $z = 0$.

A measure of the consistency of this calculation is the error in ψ_o, that is, the difference between the value of ψ at the o-point as obtained from the last 2-D calculation and that specified in the statement of the problem. In this calculation these two numbers differ by 0.4%. More iterations will not improve this number.

Figure 4a shows the contours of constant ψ for an equilibrium similar to that obtained in the proto $S - 1C$ Spheromak [13]. This field configuration, which is produced by induction from a flux core, [14] contains both poloidal and totoidal magnetic fields. The flux core has a major radius of 30 cm and a minor radius of 6 cm. In the experiment the core is enclosed by a vacuum chamber. There are external field coils outside the chamber. The boundary conditions would be difficult to simulate exactly with this code. These boundary conditions are approximated in this calculation by a outer fixed flux surface which has the same ψ value as the flux core. The top, $z = 40$, is assumed to be a fixed conductor, i.e., the ends of the flux surfaces are fixed. The external magnetic field which is simulated here has a value of 220 G.

Figure 4b is a plot of the pressure at $z = 0$, Fig. 4c is a plot of the toroidal current at $z = 0$, Fig. 4d is a plot of the poloidal magnetic field at $z = 0$, and Fig. 4e is a plot of the toroidal magnetic field at $z = 0$. The poloidal magnetic field at $r = 0$ and $z = 0$ is -1.8 kG.
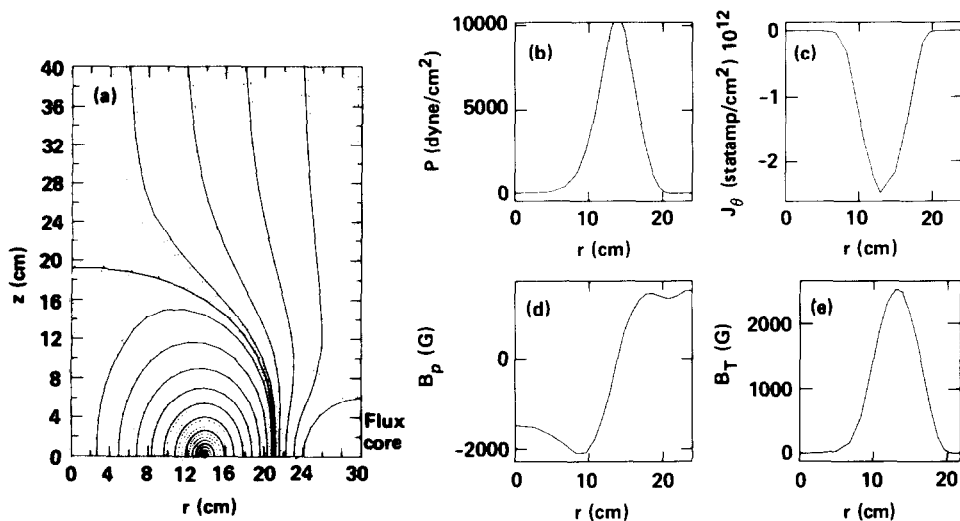
FIG. 4. Proto S — 1C equilibrium, (a) χ, λ grid, (b) pressure vs. r at $z = 0$, (c) toroidal current vs. r at $z = 0$, (d) poloidal magnetic field vs. r at $z = 0$, (e) toroidal magnetic field vs. r at $z = 0$.

In this calculation there are 9 surfaces of constant ψ inside the separatrix and 4 outside the separatrix, for a total of 14 surfaces. Each flux surface consist of 20 points. There is a total of 280 points in the 2-D grid. This calculation took about 60 1-D 2-D iterations for a total of 5.0 sec on the Cray-1. The error in the o-point value of ψ in this calculation is 0.06%.

The last example presented here is an example of an FRC, which has no toroidal magnetid field. Very elongated FRC's are produced in the field reversed theta pinch experiment FRX [6]. Figure 5a are plots of the flux surfaces of an equilibrium similar to the one in FRX. The boundary conditions used at the top, $z = 50$, is $\partial \psi / \partial z = 0$. The theta pinch coil which is 100 cm long and has a 24.8 cm i.d. forms the outer flux surface. The passive mirror is simulated by the smaller diameter at the top of Fig. 5a. This equilibrium has all the plasma enclosed by the separatrix. It is characterized by large gradient in the pressure at the separatrix, Fig. 5c, which produces a sharp peak in the toroidal current density at the separatrix, Fig. 5d. The length of the plasma, in the z direction, is controlled by the value of Q_p. Larger Q_p pushes the separatrix to higher z.

The positioning of the points on the separatrix is important in this calculation. There must be an adequate number of points in the region where the separatrix goes to $z = 0$. In this calculation instead of placing the points uniformly along the separatrix, they are spaced so that the distance between points is inversely proportional to the distance to the origin ($r = 0$, $z = 0$).

There are two approximate equilibrium conditions which characterize an FRC. The first one of these is [6],
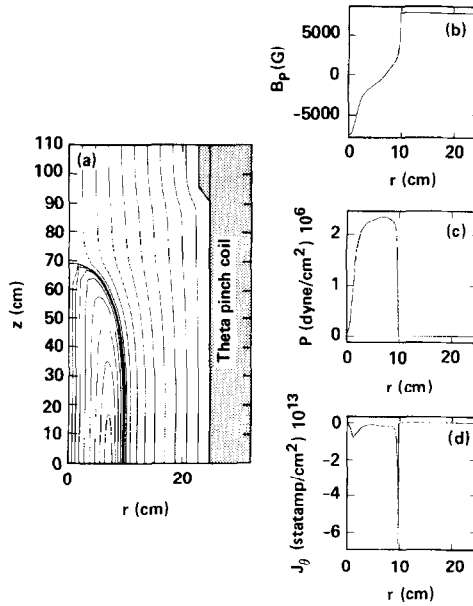
$$r_s / r_o = \sqrt{2}, \tag{28}$$

FIG. 5. FRC equilibrium, (a) χ surfaces, (b) poloidal magnetic field vs. r at $z = 0$, (c) pressure vs. r at $z = 0$, (d) toroidal current vs. r at $z = 0$.

where r_s is the separatrix radius at $z = 0$ and r_o is the radius of the o-point. In this calculation r_o is 6.990 cm and r_s is 9.840. Thus the relation (28) is satisfied to about 0.5%. The other relation is an approximate pressure balance relation [15],

$$\langle \beta \rangle = 1 - \frac{1}{2} \left(\frac{r_s}{r_w} \right)^2, \tag{29}$$

where

$$\langle \beta \rangle = \frac{1}{\pi r_s^2} \int_0^{r_s} \frac{P}{B_0^2/8\pi} \, dA, \tag{30}$$

where r_w is the radius of the wall. The above integral is over the area encircled by r_s at $z = 0$; B_0 is the magnetic field outside the separatrix at $z = 0$. For the equilibrium shown in Fig. 5, $\langle \beta \rangle$ from Eq. (29) is 0.9213 and $\langle \beta \rangle$ from Eq. (30) is 0.9188. They differ by 0.2%. Another method of checking the accuracy of this equilibrium, is to check to see if there are jumps in the quantity, $B^2/8\pi + P$, across the separatrix [17]. In this calculation this jump is approximately 1.3%.

In this calclation there are 10 flux surfaces inside the separatrix and 10 outside. Each surface is defined by 40 points. The 2-D grid consists of 800 points. This calculation took approximately 150 1-D 2-D iterations to converge for a total of 70 sec on the Cray-1. The error in the o-point is approximately 0.4%. The long thin

equilibriums are more difficult to produce then the ones with a more spherical separatrix. In this calculation the x-point is repositioned by the energy minimization method in each 1-D 2-D iteration.

REFERENCES

1. D. E. SHUMAKER, J. K. BOYD, S. P. AUERBACH, AND B. McNAMARA, *J. Comput. Phys.* **45** (1982), 266.
2. H. GRAD, "Survey of $1\frac{1}{2}$D Transport Codes," Courant Institute, New York, MF-93, 1978.
3. R. N. BYRNE AND H. N. KLEIN, *J. Comput. Phys.* **26** (1978), 352.
4. S. C. JARDIN, *J. Comput. Phys.* **42** (1981), 32.
5. A. D. TURNBULL AND R. G. STORER, *J. Comput. Phys.* **50** (1983), 409–435.
6. W. T. ARMSTRONG, R. K. LINFORD, J. LIPSON, D. A. PLATTS, AND E. G. SHERWOOD, *Phys. Fluids* **24** (1981), 2068.
7. J. DELUCIA, S. C. JARDIN, AND A. M. M. TODD, *J. Comput. Phys.* **37** (1980), 183.
8. I. B. BERNSTEIN, *Phys. Fluids* **17** (3) (1974), 547.
9. O. C. ZIENKIEWICZ, "The Finite Element Method," p. 50, 3rd ed., McGraw–Hill, New York London, 1977.
10. A. I. SHESTAKOV AND D. V. ANDERSON, *Comput. Phys. Comm.* **30** (1983), 31.
11. I. HENINS, H. W. HOIDA, T. R. JARBOE, R. K. LINFORD, J. MARSHELL, K. F. McKENNA, D. A. PLATTS, AND A. R. SHERWOOD, *in* "Proceedings of the Third Symposium on the Physics and Technology of Compact Toroids in the Magnetic Fusion Energy Program", p. 101, Los Alamos National Laboratory, Los Alamos, N. M., 1980.
12. H. W. HOIDA, J. LIPSON, I. HENINS, T. R. JARBOE, R. K. LINFORD, J. MARSHALL, D. A. PLATTS, A. R. SHERWOOD, AND M. TUSZEWSKI, *in* "Proceeding of the Fourth Symposium on the Physics and Technology of Compact Toroids," CONF-811087, p. 133, Lawrence Livermore National Laboratory, Livermore, California, 1982.
13. A. JANOS, S. COWLEY, H. HSUAN, S. PAUL, C. SKINNER, F. WYSOCKI, AND M. YAMADA, *in* "Proceeding of the Fourth Symposium on Physics and Technology of Compact Toroids," CONF-811087, p. 137, Lawrence Livermore National Laboratory, 1982.
14. S. JARDIN AND W. PARK, *Phys. Fluids* **24** (1981), 679.
15. D. C. BARNES AND C. E. SEYLER, "Proceeding of the US-Japan Joint Symposium on Compact Toruses and Energetic Particle Injection," p. 110 Princeton Univ. Princeton, N. J., 1979.
16. V. D. SHAFRANOV, *Rev. Plasma Phys.* **2** (1966), 103.
17. D. C. STEVENS, E. HAMEIRI, W. GROSSMAN, "Computation of Field-Reversed θ-Pinch Equilibria", 1983 Sherwood Theory Meeting, Arlington, Virginia, 1983.